Volume swelling of amorphous SiC during ion-beam irradiation

Manabu Ishimaru, In-Tae Bae, Akihiko Hirata, and Yoshihiko Hirotsu
The Institute of Scientific and Industrial Research, Osaka University, Ibaraki, Osaka 567-0047, Japan

James A. Valdez and Kurt E. Sickafus
Materials Science and Technology Division, Los Alamos National Laboratory, Los Alamos, New Mexico 87545, USA
(Received 17 March 2005; revised manuscript received 10 May 2005; published 25 July 2005)

Relationships between chemical short-range order and volume swelling of amorphous silicon carbide (SiC) under radiation environments have been examined using energy-filtering transmission electron microscopy in combination with imaging plate techniques. Single crystals of 4H—SiC with (0001) orientation were irradiated with 300 keV xenon ions to a fluence of 10^{15} cm^{-2} at cryogenic (120 K) and elevated (373 K) temperatures. A continuous amorphous layer was formed in both specimens, but the magnitude of their volume change was different: volume swelling becomes more pronounced with decreasing irradiation temperatures. From radial distribution function analyses, it was found that the amount of Si—Si atomic pairs increases more rapidly than that of C—C atomic pairs with the progress of chemical disordering. We discuss the ion-beam-induced swelling in amorphous SiC within the context of our results as well as previous observations.

DOI: 10.1103/PhysRevB.72.024116 PACS number(s): 61.43.Dq, 61.14.Lj, 61.82.Fk

I. INTRODUCTION

When materials are subjected to radiation with energetic particles such as neutron, ion, and electron, their atomistic structures are altered: atoms may switch positions with each other, or even be removed from their lattice sites. The accumulation of these defects leads to degradation of the material, and ultimately induces amorphization. Amorphization often gives rise to significant volume changes and concomitant microcracking. Understanding the response of materials under radiation environments is, therefore, of technological importance to predict material performance for nuclear applications.

Silicon carbide (SiC) and its composites have been proposed for structural components in future nuclear fusion reactors,[1,2] because of their high temperature strength, pseudoductile fracture behavior, and low-induced radioactivity. To obtain knowledge regarding radiation effects in SiC, extensive studies are still continued in both experimental and theoretical approaches. Especially, volume swelling of this material was examined by various techniques, such as Rutherford backscattering spectroscopy,[3,4] surface profilometry,[3] electron energy-loss spectroscopy (EELS),[4–6] and molecular-dynamics (MD) approach.[7,8] As a consequence, it is reported that the volume of crystalline SiC increases with damage accumulation up to amorphization. However, the magnitude of swelling reported so far is highly scattered from 8 to 20%.[3–7,9–11] These motivated us to study volume swelling of amorphous SiC generated by irradiations.

Höfgen *et al.*[12] examined the annealing behavior of amorphous SiC using profilometry and x-ray diffraction, and observed large volume reduction (so-called "densification") of amorphous SiC prior to crystallization. We have recently investigated atomistic structures of amorphous SiC using conventional transmission electron microscopy (TEM).[13] The radial distribution functions obtained by electron diffraction revealed that amorphous SiC networks contain not only heteronuclear (Si—C) bonds but also homonuclear (Si—Si and C—C) bonds within the first coordination shell, and their structures alter upon annealing which is referred to as structural relaxation. These results suggest that amorphous SiC is not a single structure, but there is a variety of chemical short-range order that can be described by the ratio of the heteronuclear to homonuclear bonds. Based on these results, we speculated that the scattered magnitude of swelling originates from the difference of amorphous structures. In the present study, we examined ion-beam-induced amorphous structures of SiC using advanced electron microscopy techniques, and discussed the relationships between chemical short-range order and volume swelling of amorphous SiC.

This paper is organized as follows: The experimental procedures including ion irradiation conditions and TEM observations are described in Sec. II. In Sec. III, volume swelling and atomic pair-distribution functions are examined as a function of irradiation temperatures. In Sec. IV, we discuss the ion-beam-induced volume swelling in amorphous SiC within the context of our results as well as previous observations. Finally, we present our conclusions in Sec. V.

II. EXPERIMENTAL PROCEDURES

Single crystalline *p*-type 4H—SiC wafers obtained from Nippon Steel Corporation were used in this study. The surface was normal to the [0001] crystallographic axis, and polished to an optical grade finish. All specimens for irradiation experiments were cut from the same substrate to avoid any possible effects of initial crystallinity on amorphous structures. Then, the specimens were irradiated at cryogenic (120 K) and elevated temperatures (373 K) with 300 keV xenon (Xe) ions using an ion implanter in the Ion Beam Materials Laboratory at Los Alamos National Laboratory. The ion fluence was fix to 10^{15} Xe/cm^2 and the average ion flux was maintained at $\sim 2 \times 10^{12}$ Xe/cm^2 s during the irradiation, so the effects of impurity atoms and beam-heating on amorphous structures are the same between both specimens. The substrates were tilted $\sim 5°$ from the direction of the incident ion beam in order to reduce ion-channeling effects.

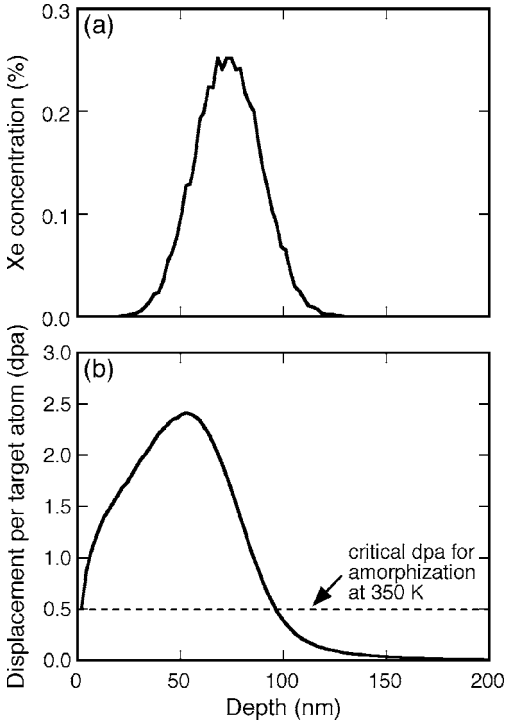

FIG. 1. Monte Carlo simulation results for the spatial distribution of (a) Xe projectiles and (b) damage created by 300 keV Xe ions to a fluence of 10^{15} cm^{-2} in 4H—SiC. For the TRIM calculation, it was assumed that the threshold displacement energies of silicon and carbon correspond to 35 and 20 eV, respectively.

According to TRIM calculations,[14] the maximum concentration of Xe was approximately 0.25% under the present irradiation conditions [Fig. 1(a)]. The instantaneous damage was 2.4 dpa (displacement per target atom) at the peak maximum of the damage profile [Fig. 1(b)], which is higher than the critical dpa of 0.5 for amorphization of SiC at 350 K with 1.5 MeV Xe ion irradiation.[15]

Cross-sectional samples for TEM observations were prepared by gluing an unirradiated SiC sample to the surface of the irradiated SiC, cutting cross sections of the sample (perpendicular to the irradiated surface), and using a tripod polishing technique to thin the specimens prior to argon ion milling (the glancing angle of argon ions was as low as 4°). The acceleration voltage for ion milling was initially set to 4 keV (GATAN, PIPS) and was finally decreased to 0.25 keV (Technoorg-Linda Co., Gentle Mill) in order to minimize radiation damage induced by argon ions. Irradiation-induced-microstructures were observed at an incident electron energy of 300 kV using a JEOL JEM-3000F TEM.

Generally, two types of electrons contribute to the formation of electron diffraction patterns: one is elastically-scattered electrons, and the other is inelastically-scattered electrons. The latter enhance the background intensity, and therefore it degrades a quantitative analysis of electron diffraction intensity. To remove the inerastically-scattered electrons, we employed an energy-filtering TEM, Carl Zeiss LEO-922D TEM equipped with an in-column-type energy-filter, operated at 200 kV. Electron diffraction patterns were recorded on imaging plates that have a higher degree of linearity and a wider dynamic range in recording electron intensities as compared with conventional TEM films.[16] The intensities of the halo patterns were digitized quantitatively using an imaging plate processor, a Digital Micro-Luminography FDL-5000 system (Fuji Film). The details of the electron diffraction analysis are described elsewhere.[17,18]

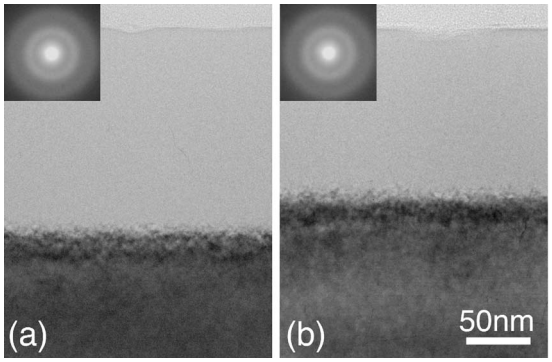

FIG. 2. Cross-sectional bright-field images of the specimens irradiated at (a) cryogenic and (b) elevated temperatures. The corresponding electron diffraction patterns are indicated as the inset. The thickness of the amorphous layer in (b) is smaller than that in (a), suggesting that *in situ* damage-annealing takes place.

III. RESULTS

Figure 2 shows cross-sectional bright-field TEM images and the corresponding electron diffraction patterns obtained from the ion-beam-induced layers of specimens irradiated at (a) cryogenic and (b) elevated temperatures. The halo diffraction patterns of Figs. 2(a) and 2(b) reveal that complete amorphization occurs in both specimens. The bright-field images show that the thickness of amorphous layer is ~150 nm in Fig. 2(a), while it is ~120 nm in Fig. 2(b). The formation of the thinner amorphous layer in Fig. 2(b) indicates the occurrence of the damage-recovery during ion irradiation due to the higher irradiation temperature. This *in situ* damage annealing results in the different chemical short-range ordered states between both specimens, as described below.

Volume swelling as a function of irradiation temperatures was examined using EELS. Figure 3 reveals low-loss EELS spectra of amorphous SiC generated by the irradiation at cryogenic and elevated temperatures. Also shown in Fig. 3 is an EELS spectrum obtained from a pristine 4H—SiC substrate. All EELS spectra were taken on the same day, because there is a possibility that they are affected by the external conditions.[5] In addition to a zero-loss peak due to the elastically-scattered electrons, a prominent peak corresponding to plasmon energy, E_p, can be seen around 20 eV. The plasmon-loss peak is located at E_p(pristine)=22.0 eV for crystalline SiC, while it moves to the lower energy side in amorphous SiC: the plasmon energy decreases with the damage accumulation. A similar redshift in plasmon energy was also observed in a crystalline-to-amorphous phase transformation induced by electron-beam[5] and ion-beam[6,19] irradiations. The plasmon energy is proportional to the square root

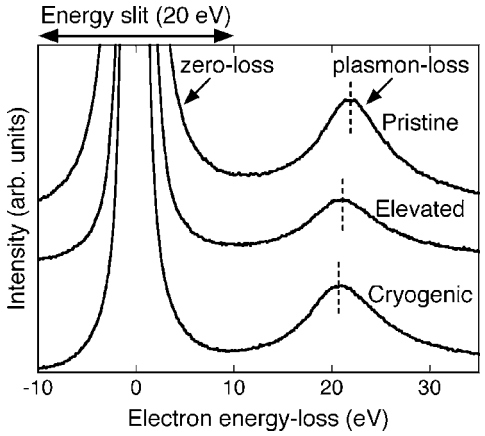

FIG. 3. Low-loss EELS spectra of crystalline and amorphous SiC. Besides a zero-loss peak due to the elastically-scattered electrons, a plasmon-loss peak exists around 20 eV. The plasmon-loss peak shows redshift of 0.9 and 1.3 eV for amorphous SiC generated by irradiation at elevated and cryogenic temperatures, respectively, relative to the pristine crystal.

of the number density of valence electrons,[20] and therefore its value is related to the density of amorphous SiC if the average number of nearly free electrons is assumed to be four per atom. On the basis of this assumption, the plasmon energies of 22.0, 21.1, and 20.7 eV correspond to the densities of 2.93, 2.70, and 2.59 g/cm^3, respectively. It should be noted that the value of 2.93 g/cm^3 is smaller than that of crystalline SiC (3.21 g/cm^3). The volume swelling estimated from $[E_p(\text{pristine})/E_p]^2-1$ (Ref. 4) is equal to 8.7% for the sample irradiated at an elevated temperature and 13.0% for that irradiated at a cryogenic temperature, which are in agreement with previous investigations.[3–7,10,11] Our present results indicate that the magnitude of volume swelling depends on the irradiation conditions, and help to explain the highly scattered values reported previously.

The density change observed by EELS measurements suggests the alteration of amorphous structures upon irradiation. In fact, on a close examination of the halo diffraction patterns, we further found that the halo rings obtained from the specimen irradiated at a cryogenic temperature [Fig. 2(a)] are more diffuse than those from the specimen irradiated at an elevated temperature [Fig. 2(b)]. In order to investigate short-range order of amorphous SiC, the intensities of the halo diffraction patterns were analyzed quantitatively using energy-filtering TEM in combination with imaging plate techniques. Electron diffraction intensities are highly susceptible to modification by dynamical effects such as multiple scattering.[21] The specimen thickness t can be estimated from an EELS spectrum using the following equation: $t/\lambda_p = \ln(I_T/I_0)$, where λ_p is the plasmon mean-free path, I_T the total intensity in the spectrum, and I_0 the intensity under the zero-loss peak.[20] In order to optimize structural analyses of amorphous regions, we obtained electron diffraction patterns from thin-foil regions with $t/\lambda_p \sim 0.25$. In recording halo patterns, amorphous layers were selected using an electron probe with a size of ~100 nm. The parallelity of the incident electron beam in this condition was $\sim 8\times 10^{-5}$ rad, which is parallel enough for the electron-beam radial distribution analysis.[17]

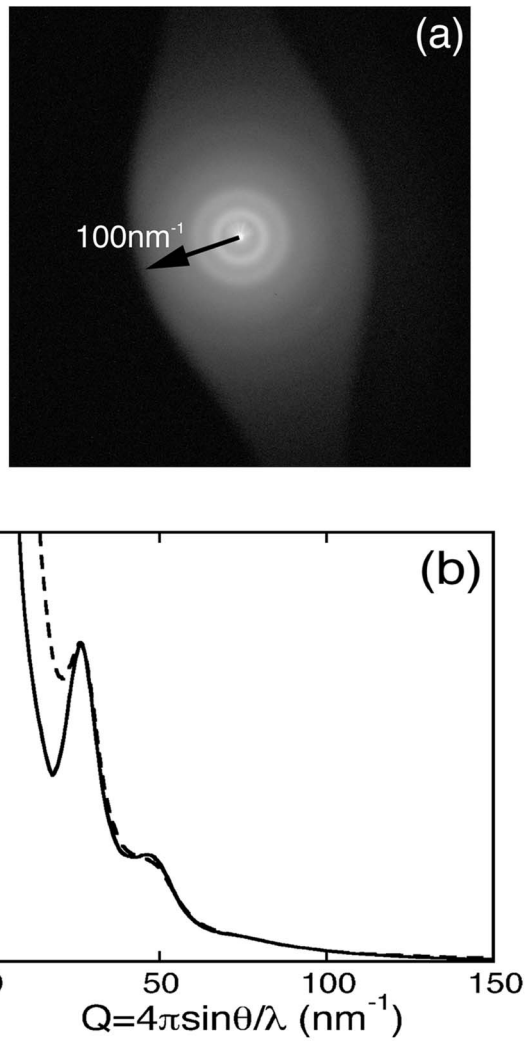

FIG. 4. (a) Energy-filtered electron diffraction pattern of amorphous SiC and (b) its intensity profile (solid line). An intensity profile obtained by conventional TEM is also indicated by broken line in (b). For comparison, the intensities are normalized at the first halo peak. The inelastically scattered electrons are successfully removed by using energy-filtering TEM.

An example of energy-filtered diffraction pattern of amorphous SiC is displayed in Fig. 4(a). This pattern was taken by inserting an energy slit of 20 eV (plus minus 10 eV) (see Fig. 3). The position of a plasmon-loss peak is approximately 20 eV, and therefore most of the inelastically-scattered electrons can be removed under the present condition. From the electron diffraction pattern of Fig. 4(a), one dimensional electron intensity profile, $I(Q)$, averaged in the radial direction in the reciprocal-lattice space, was obtained as a function of the scattering vector, Q.[22] The scattering vector is expressed as $Q=4\pi \sin\theta/\lambda$, where θ is the half-scattering angle and λ is the electron wavelength, and the camera length was corrected using Bragg reflections from the 4H—SiC substrate. The resulting $\langle I(Q)\rangle$ is indicated by a solid line in Fig. 4(b). A dashed line also shown in Fig. 4(b) corresponds to the $\langle I(Q)\rangle$ of a conventional (unfiltered) diffraction pattern. It is clearly seen that the background inten-

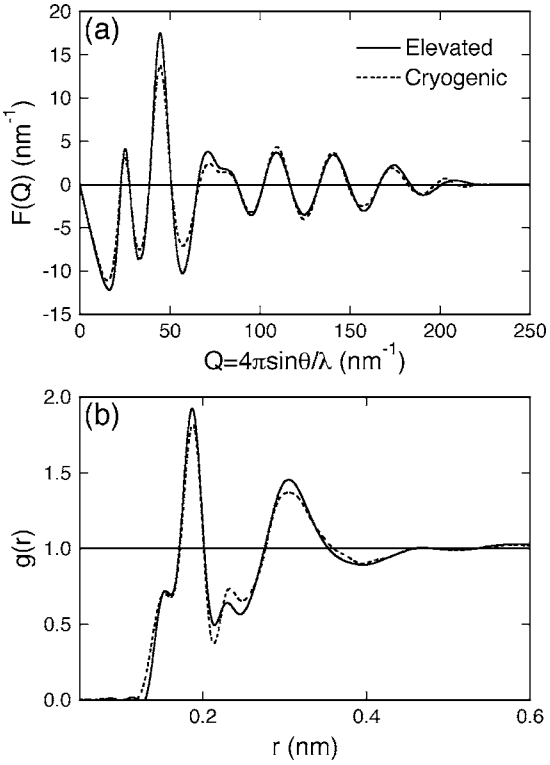

FIG. 5. (a) The experimentally measured reduced interference functions, $S(Q)$, and (b) atomic pair-distribution functions, $g(r)$. Solid and dashed lines correspond to the samples irradiated at elevated and cryogenic temperatures, respectively. In the $g(r)$, with decreasing the irradiation temperature the peak associated with the Si—Si bonds increases more rapidly than that associated with the C—C bonds.

sity within 80 nm^{-1} is successfully removed by using energy-filtering TEM, suggesting that inelastically-scattered electrons due to plasmon-loss and core-loss are successfully removed. The intensity profile above 80 nm^{-1} is almost the same between the filtered and unfiltered diffraction patterns, and therefore the whole intensity profile was obtained by connecting both profiles at 100 nm^{-1}.

Reduced interference functions, $F(Q)=Q[S(Q)-1]$, where $S(Q)$ is the structure factor for the electron diffraction intensities, were obtained by subtracting a smooth cubic spline curve for background which penetrates through the halo intensity ripples of $\langle I(Q)\rangle$ along Q. In Fig. 5(a) is shown $F(Q)$ for the samples irradiated at cryogenic (dashed line) and elevated (solid line) temperatures. The peak height in the $F(Q)$ obtained here is more pronounced than that obtained by conventional TEM (cf. as-irradiated sample of Fig. 2 in Ref. 13), suggesting the usefulness of energy-filtering TEM. Very weak intensity profiles up to high scattering angles as high as $Q=220$ nm^{-1} are recorded well above the background intensity level of the imaging plate. The maximum scattering vector in the present study is much higher than ~150 (Ref. 23) and ~160 nm^{-1} (Ref. 24) obtained in previous x-ray and electron diffraction studies. This means that we can obtain a higher spatial resolution in the real lattice space as compared to the previous diffraction experiments. In the $F(Q)$, it is readily noticed that the oscillation of intensity profiles is more pronounced in the specimen irradiated at an elevated temperature as compared with that irradiated at a cryogenic temperature.

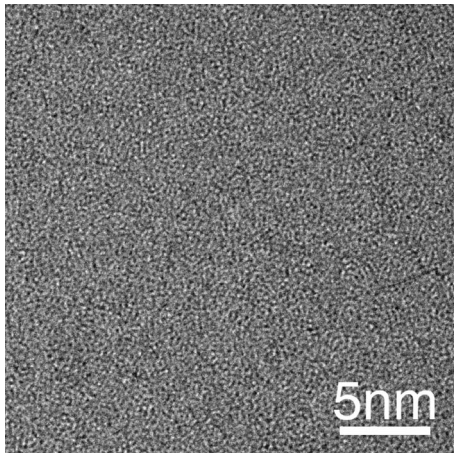

FIG. 6. High-resolution TEM image of amorphous SiC induced by irradiation at a cryogenic temperature. No detectable clusters and phase-separated regions were observed.

Reduced radial distribution functions, $G(r)$, were extracted by the Fourier transform of $F(Q)$. $G(r)$ is expressed as $4\pi r\rho_0\{g(r)-1\}$, where ρ_0 is the average density of the sample and $g(r)$ is the atomic pair-distribution function which is the probability of finding another atom at a distance between r to $r+\Delta r$ from a specific atom. The $g(r)$ of amorphous SiC generated by the irradiation at cryogenic (broken line) and elevated (solid line) temperatures is shown in Fig. 5(b). Prominent peaks appear at ~0.19 and ~0.31 nm which can be compared with the first and second nearest neighbors of crystalline SiC, respectively. In addition to these peaks, subpeaks appear on either side of the first prominent Si—C peak in Fig. 5(b). The r positions of these peaks, ~0.15 and ~0.23 nm, can be assigned to C—C and Si—Si bond lengths, respectively. This suggests that amorphous SiC networks contain not only heteronuclear bonds but also homonuclear bonds, as reported previously.[5–8,13,25–28] The peaks associated with the homonuclear bonds are not caused by macroscopic clustering or phase separation, because there are no halo rings and intensities due to amorphous silicon and carbon in electron diffraction patterns and $F(Q)$ [see Figs. 2 and 5(a)]. In fact, high-resolution TEM images (Fig. 6) reveal a typical salt and pepper contrast and no detectable clusters and phase-separated regions exist.

The locations of the first and second nearest neighbor peaks are almost the same between the specimens irradiated at cryogenic (broken line) and elevated (solid line) temperatures. On the other hand, the ratio of the heteronuclear to homonuclear bonds depends on the ion implantation conditions. With increasing the irradiation temperature the peak associated with the heteronuclear Si—C bond (~0.19 nm) becomes more pronounced, whereas the peaks corresponding to homonuclear Si—Si and C—C bonds (~0.15 and ~0.23 nm) simultaneously decrease. It means that the amorphous structures of the sample irradiated at a cryogenic temperature are more chemically disordered than those of the sample irradiated at an elevated temperature. This result is

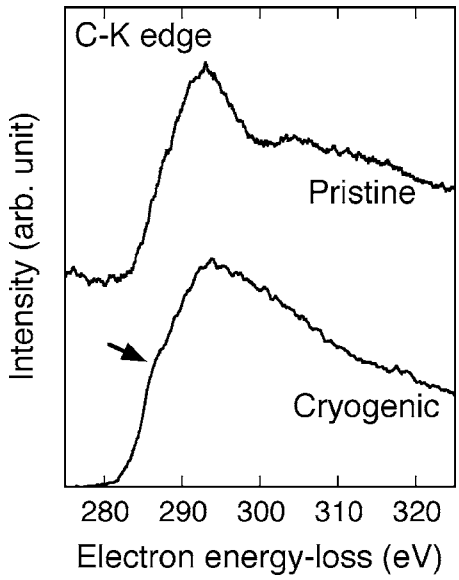

FIG. 7. Core-loss EELS spectrum of carbon in amorphous SiC generated by irradiation at a cryogenic temperature. For comparison, the C-*K* edge EELS spectrum of crystalline 4H—SiC is also indicated. A shoulder due to sp^2 bonding is indicated by an arrow.

quite reasonable, since the damage-recovery-rate during irradiation (*in situ* damage-annealing) increases with the irradiation temperature.

IV. DISCUSSION

Until now, several atomistic models have been proposed for volume swelling associated with amorphization.[5,7,8,29,30] Muto and Tanabe[5] examined amorphous structures of electron-irradiated SiC using partial pair-distribution functions extracted from the extended energy-loss fine structure of EELS spectra. They found that amorphous SiC networks consist of Si—Si (bond length: 0.235 nm), Si—C (0.189 nm), and sp^3 C—C (0.154 nm) covalent bonds within the first coordination shell, and proposed that the significant volume swelling associated with amorphization is due to the increase in the average bond length in addition to the conventional void swelling. To confirm the chemical bonding state of carbon, we measured its core-loss spectrum. The C-*K* edge EELS spectrum of amorphous SiC induced by the irradiation at a cryogenic temperature is indicated in Fig. 7, together with that of crystalline 4H—SiC. Backgrounds, I_B, in Fig. 7 are subtracted using the power low model, $I_B = AE^{-r}$, where A and r are fitting parameters.[20] Only the $1s \rightarrow \sigma^*$ transition is visible in crystalline SiC, while a shoulder corresponding to the $1s \rightarrow \pi^*$ transition is apparent at 286 eV in amorphous SiC. The existence of sp^2 C—C bonds were also observed in amorphous SiC generated by aluminum-implantation into 4H—SiC (Ref. 6) and carbon-implantation into amorphous Si.[26] The discrepancy between the electron and ion irradiations is presumably due to the different amorphization processes. That is, an electron beam produces simple point defects such as Frenkel pairs, while extensive damage regions, so-called cascade, are formed along the ion trajectories.

On the basis of the results obtained by MD simulations, Yuan and Hobbs[8] and Gao and Weber[7] proposed that the homonuclear bonds play an important role for swelling of crystalline SiC during the damage accumulation. As described above, we found that the ratio of the heteronuclear to homonuclear bonds in amorphous SiC networks depends on the ion implantation conditions. It should be noted that with decreasing the irradiation temperature the peak associated with the Si—Si bonds (~0.23 nm) is more pronounced than that associated with the C—C bonds (~0.15 nm). This means that the amount of the longer bond increases with chemical disordering; the average bond length becomes large. The preferential formation of Si—Si atomic pairs is also observed in damaged crystalline SiC (Refs. 5 and 6) and amorphous SiC.[31] On the contrary, Si—Si atomic pairs decreases more rapidly than C—C ones in structural relaxation processes.[13] We propose that the difference of the formation and annihilation speeds between the homonuclear bonds results in the significant volume changes under radiation environments and upon thermal annealing. The volume change of SiC under electron-beam irradiation has been also ascribed to an availability of homonuclear bonds.[5] In this model the lack of sp^2 C—C covalent bonds is one of the important factors, while our present study revealed the existence of both sp^2 and sp^3 C—C atomic pairs. Moreover, the formation rate of the homonuclear bonds is not considered in the previous model. From this viewpoint, the mechanism of volume swelling proposed by us is essentially different from that reported in Ref. 5.

To confirm if there exists the unbalance of the formation rate between Si—Si and C—C atomic pairs, partial coordination numbers, N_{ij}, of amorphous SiC were examined by MD simulations utilizing the Tersoff interatomic potential.[32,33] Gao and Weber[34] performed MD simulations of ion irradiation into SiC, and reported that amorphous structures generated by cascade overlap are similar to those obtained by melt-quenching. In the present study, therefore, we prepared amorphous SiC networks by rapid quenching from the liquid state and annealed them in order to obtain different chemical short-range ordered states.[13,35] Table I shows the N_{ij} of as-quenched and annealed samples, which correspond to lesser and greater chemical order, respectively. The N_{ij} gives the average number of j-type neighbors for the i-type atom within the first coordination shell in the partial atomic pair-distribution function. It is apparent that the N_{SiSi} value is larger than the N_{CC} one, and the former decreases rapidly than the latter as chemical order develops. This is attributed to the difference of the bond energy between Si—Si (2.32 eV/bond) and C—C (3.68 eV/bond). The behavior of the N_{ij} associated with the change of chemical short-range order is consistent with the experimental result obtained here, suggesting the validity of the present study. As far as we know, the present study is the first to provide the existence of the unbalance formation speed between Si—Si and C—C atomic pairs during structural changes of amorphous SiC.

We estimated how much volume swelling occurs due to the unbalance formation rate in the homonuclear bonds. The experimentally-measured $G(r)$ was simply integrated, since electron diffraction cannot extract partial radial distribution

TABLE I. Partial coordination numbers, N_{ij}, of amorphous SiC generated by MD simulations. Tersoff-89 and Tersoff-94 denote the interatomic potential proposed by Tersoff on 1989 and 1994, respectively. As-quenched and annealed SiC correspond to the amorphous network with lesser and greater chemical short-range order. As chemical order progresses, the amount of heteronuclear bonds increases, while that of homonuclear bonds decreases. It should be noted that the N_{SiSi} increases more rapidly than the N_{CC} with chemical disordering (see "variation").

	Tersoff-89			Tersoff-94		
	N_{CC}	N_{SiC}	N_{SiSi}	N_{CC}	N_{SiC}	N_{SiSi}
as-quenched	1.33	2.16	2.34	1.33	2.66	1.87
annealed	1.25	2.27	2.14	1.30	2.70	1.75
(variation)	(−0.08)	(+0.11)	(−0.20)	(−0.03)	(+0.04)	(−0.12)

functions, unlike x-ray diffraction and neutron diffraction. The partial coordination numbers of the sample irradiated at a cryogenic (elevated) temperature are 2.67 (2.67) for the C—C peak, 4.48 (5.19) for the Si—C one, and 2.95 (2.28) for the Si—Si one. Strictly speaking, the Si—C and Si—Si peaks overlap with other peaks such as the second peak of the C—C bonding. Moreover, the coordination number of the C—C atomic pairs is overestimated due to the dynamical effects such as multiple scattering,[21] as described above. The electron diffraction patterns were taken from the region with almost the same thickness, and therefore we discuss here only the relative difference of the density between amorphous SiC generated by the irradiation at elevated and cryogenic temperatures. From the arithmetic mean of covalent bond lengths and partial coordination numbers, the volume difference between both specimens was found to be approximately 5%, which is in good agreement with that estimated from the plasmon energy (4.3%).

Finally, we discuss the effects of topological and chemical short-range order on volume swelling. It is known that the volume changes also occur in other Si-based materials. Amorphous Si prepared by low-energy[36] (high-energy[37]) self-implantation is determined to be 3.1% (1.8%) less dense than crystalline Si. Laaziri, Roorda, and Baribeau[38] measured the atomic density of amorphous silicon-germanium ($Si_{1-x}Ge_x$) alloys prepared by high-energy ion implantation into single-crystalline $Si_{1-x}Ge_x$ layers, deposited epitaxially on Si substrates. Their Rutherfold backscattering spectroscopy and surface profilometry measurements revealed that the density of amorphous $Si_{1-x}Ge_x$ alloys is 1.5–2.1 % lesser than that of crystalline states. These values are apparently smaller than those observed in SiC (8–20 %). In the case of amorphous Si, no chemical disorder exists. On the other hand, it is reported that amorphous $Si_{1-x}Ge_x$ alloys possess the random mixing of Si and Ge atoms at the first coordination shell, so-called complete chemical disorder.[39,40] We have recently examined amorphous structures of $Si_{1-x}Ge_x$ alloys as well as their structural relaxation processes.[41,42] As a consequence, it was found that chemical disorder is almost the same between the as-quenched and annealed amorphous $Si_{1-x}Ge_x$ alloys, whereas the reduction of topological disorder is observed upon annealing: structural changes in immiscible amorphous $Si_{1-x}Ge_x$ networks can proceed with the alternation of topological short-range order only. These results suggest that complete chemical disorder ($Si_{1-x}Ge_x$) or no chemical disorder (Si) result in smaller volume changes as compared with SiC. In fact, a previous MD simulations pointed out that almost 80% of the density change on amorphization in SiC is due to chemical disorder rather than topological disorder.[8]

V. CONCLUSIONS

We examined atomistic structures and volume swelling of amorphous SiC generated by ion-beam-bombardment using energy-filtering TEM. The following results are obtained.

(1) The plasmon-loss peak shows redshift of 0.9 and 1.3 eV for amorphous SiC generated by irradiation at elevated and cryogenic temperatures, respectively, relative to the pristine crystal. This indicates that the volume swelling of amorphous SiC becomes more pronounced with decreasing the irradiation temperature.

(2) The amorphous SiC networks consist of Si—Si (bond length: ~0.23 nm), Si—C (~0.19 nm), and C—C (~0.15 nm) covalent bonds within the first coordination shell. The ratio of heteronuclear to homonuclear bonds is found to depend on the irradiation conditions: with increasing the irradiation temperature the peak associated with the heteronuclear Si—C bond becomes more pronounced, whereas the peaks corresponding to homonuclear Si—Si and C—C bonds simultaneously decrease.

(3) The partial coordination number of Si—Si atomic pairs is larger than that of C—C atomic pairs, and the former increases rapidly than the latter with decreasing the irradiation temperature: the average bond length becomes large with the progress of chemical disordering. The difference of the formation speed between the homonuclear bonds is attributed to the significant volume swelling under radiation environments. Highly scattered magnitude of swelling reported so far is attributed to the difference of chemical short-range ordered state in amorphous SiC networks.

ACKNOWLEDGMENTS

We would like to thank J. R. Tesmer for his assistance with ion implantations. This research was partially supported by the 21st century Center of Excellence program "Towards

Creating New Industries Based on Inter-Nanoscience" and the Grant-in-Aid for Scientific Research on Priority Areas (No. 15074212) from the Ministry of Education, Culture, Sports, Science, and Technology, Japan. Funding by the U.S. Department of Energy, Office of Basic Sciences, Division of Materials Sciences is also acknowledged.

[1] L. H. Rovner and G. R. Hopkins, Nucl. Technol. **29**, 274 (1976).
[2] R. H. Jones, L. Giancarli, A. Hasegawa, Y. Katoh, A. Kohyama, B. Riccardi, L. L. Snead, and W. J. Weber, J. Nucl. Mater. **307–311**, 1057 (2002).
[3] R. Nipoti, E. Albertazzi, M. Bianconi, R. Lotti, G. Lulli, M. Cervera, and A. Carnera, Appl. Phys. Lett. **70**, 3425 (1997).
[4] W. Jiang, C. M. Wang, W. J. Weber, M. H. Engelhard, and L. V. Saraf, J. Appl. Phys. **95**, 4687 (2004).
[5] S. Muto and T. Tanabe, J. Appl. Phys. **93**, 3765 (2003).
[6] C. W. Wang, Y. Zhang, W. J. Weber, W. Jiang, and L. E. Thomas, J. Mater. Res. **18**, 772 (2003).
[7] F. Gao and W. J. Weber, Philos. Mag. **85**, 509 (2005).
[8] X. L. Yuan and L. W. Hobbs, Nucl. Instrum. Methods Phys. Res. B **191**, 74 (2002).
[9] C. J. McHargue and J. M. Williams, Nucl. Instrum. Methods Phys. Res. B **80/81**, 889 (1993).
[10] V. Heera, J. Stoemenos, R. Kögler, and W. Skorupa, J. Appl. Phys. **77**, 2999 (1995).
[11] L. L. Snead and J. C. Hay, J. Nucl. Mater. **273**, 213 (1999).
[12] A. Höfgen, V. Heera, F. Eichhorn, and W. Skorupa, J. Appl. Phys. **84**, 4769 (1998).
[13] M. Ishimaru, I.-T. Bae, Y. Hirotsu, S. Matsumura, and K. E. Sickafus, Phys. Rev. Lett. **89**, 055502 (2002).
[14] J. F. Ziegler, J. P. Biersack, and U. Littmark, *The Stopping and Range of Ions in Solids* (Pergamon, New York, 1985).
[15] W. J. Weber, L. M. Wang, and N. Yu, Nucl. Instrum. Methods Phys. Res. B **116**, 322 (1996).
[16] N. Mori, T. Oikawa, T. Katoh, J. Miyahara, and Y. Harada, Ultramicroscopy **25**, 195 (1988).
[17] Y. Hirotsu, T. Ohkubo, I.-T. Bae, and M. Ishimaru, J. Electron Microsc. **50**, 435 (2001).
[18] T. Ohkubo and Y. Hirotsu, Phys. Rev. B **67**, 094201 (2003).
[19] K. Hojo, S. Furuno, K. N. Kushita, H. Otsu, Y. Furuya, and K. Izumi, Nucl. Instrum. Methods Phys. Res. B **116**, 382 (1996).
[20] For example, see D. B. Williams and C. B. Carter, *Transmission Electron Microscopy* (Plenum Press, New York, 1996).
[21] For example, see P. Hirsch, A. Howie, R. B. Nicholson, D. W. Pashley, and M. J. Whelan, *Electron Microscopy of Thin Crystals* (Robert E. Krieger Publishing Co., Inc., New York, 1977).
[22] We took some electron diffraction patterns with different exposure times, and confirmed that their intensity profiles are almost the same: the electron beam damage in the present materials during the exposures is negligible.
[23] J. Bentley, P. Angelini, A. P. Gove, P. S. Sklad, and A. T. Fisher, Inst. Phys. Conf. Ser. **98**, 107 (1989).
[24] C. Meneghini, S. Pascarelli, F. Boscherini, S. Mobilio, and F. Evangelisti, J. Non-Cryst. Solids **137/138**, 75 (1991).
[25] F. Finocchi, G. Galli, M. Parrinello, and C. M. Bertoni, Phys. Rev. Lett. **68**, 3044 (1992).
[26] C. Serre, L. Calvo-Barrio, A. Pérez-Rodríguez, A. Romano-Rodríguez, J. R. Morante, Y. Pacaud, R. Kögler, V. Heera, and W. Skorupa, J. Appl. Phys. **79**, 6907 (1996).
[27] W. Bolse, Nucl. Instrum. Methods Phys. Res. B **148**, 83 (1999).
[28] V. I. Ivashchenko, P. E. A. Turchi, V. I. Shevchenko, L. A. Ivashchenko, and G. V. Rusakov, Phys. Rev. B **66**, 195201 (2002).
[29] J. Li, J. Appl. Phys. **95**, 6466 (2004).
[30] A. Romano, M. Bertolus, M. Defranceschi, and S. Yip, Nucl. Instrum. Methods Phys. Res. B **202**, 100 (2003).
[31] M. Ishimaru, I.-T. Bae, and Y. Hirotsu, Phys. Rev. B **68**, 144102 (2003).
[32] J. Tersoff, Phys. Rev. B **39**, 5566 (1989); **41**, 3248 (1990); **49**, 16349 (1994).
[33] The validity of the Tersoff potential for covalent materials is described in the following articles: M. Ishimaru, K. Yoshida, and T. Motooka, Phys. Rev. B **53**, 7176 (1996); M. Ishimaru, K. Yoshida, T. Kumamoto, and T. Motooka, Phys. Rev. B **54**, 4638 (1996); M. Ishimaru, S. Munetoh, and T. Motooka, Phys. Rev. B **56**, 15133 (1997); M. Ishimaru, J. Appl. Phys. **91**, 686 (2002).
[34] F. Gao and W. J. Weber, J. Appl. Phys. **89**, 4275 (2001).
[35] MD simulations were performed under the isovolume condition: the density of the MD cell was fixed to 3.0 g/cm^3.
[36] P. K. Giri, V. Raineri, G. Franzo, and E. Rimini, Phys. Rev. B **65**, 012110 (2001).
[37] J. S. Custer, M. O. Thompson, D. C. Jacobson, J. M. Poate, S. Roorda, W. C. Sinke, and F. Spaepen, Appl. Phys. Lett. **64**, 437 (1994).
[38] K. Laaziri, S. Roorda, and J. M. Baribeau, J. Non-Cryst. Solids **191**, 193 (1995).
[39] L. Incoccia, S. Mobilio, M. G. Proietti, P. Fiorini, C. Giovannella, and F. Evangelisti, Phys. Rev. B **31**, 1028 (1985).
[40] A. Filipponi, P. Fiorini, F. Evangelisti, A. Balerna, and S. Mobilio, J. Phys. (Paris) **47**, 357 (1986).
[41] M. Ishimaru, M. Yamaguchi, and Y. Hirotsu, Phys. Rev. B **68**, 235207 (2003).
[42] M. Ishimaru, M. Yamaguchi, and Y. Hirotsu, Jpn. J. Appl. Phys., Part 1 **43**, 7966 (2004).